

Significant dependence of the efficiency of energy-saving thermochromic VO₂ on slight changes of its properties in the visible due to strain and/or vacancies

Jiri Houska

Department of Physics and NTIS - European Centre of Excellence, University of West Bohemia, Univerzitni 8, 30614 Plzen, Czech Republic, email jhouska@kfy.zcu.cz

Abstract

There are worldwide efforts to maximize the energy saving achieved by VO₂-based thermochromic coatings. In particular, there are very different values of the modulation of integral solar energy transmittance, reported by various laboratories on various templates even for seemingly very similar coatings. A detailed analysis reveals that this is largely due to the combination of the intentional and well understood transmittance modulation in the infrared (always beneficial) with not yet understood slight transmittance modulation in the visible (sometimes beneficial, sometimes harmful, and always multiplied by strong solar irradiance). Ab-initio calculations are used to examine the hypothesis that the transmittance modulation in the visible can be controlled by lattice strain and/or slightly off-stoichiometric [O]/[V] ratio. The presented phenomenon opens a pathway which may lead, in a case of reproducible preparation of correctly altered VO₂, to significantly enhanced energy saving.

Keywords

Vanadium dioxide; Thermochromic films; Smart windows; Reactive sputtering; Ab-initio calculations; Optical constants

1. Introduction

Vanadium dioxide is presently the most investigated thermochromic material. Its two key polymorphs include the low-temperature semiconductive monoclinic (distorted rutile) phase VO₂(M1), and the high-temperature metallic tetragonal (perfect rutile) phase VO₂(R) [1]. Thus, heating of VO₂ above its transition temperature (T_{tr}) leads to closing of the narrow band gap, to orders of magnitude higher concentration of free charge carriers, and to a strong modulation of all properties which the charge carriers are responsible for. This includes enhanced extinction coefficient especially in the infrared, enhanced electrical conductivity or enhanced electronic part of thermal conductivity. The modulation of functional properties can be used in many applications, including, probably in the first place, energy-saving smart windows which transmit infrared radiation in the cold state but reflect a significant part of infrared radiation in the hot state. See the recent reviews [2-8].

The research in this field [9-38] is focused on two groups of challenges. First, we need the ability to prepare the desired material at all, ideally by a technique (such as magnetron sputtering) which is really used in large industrial glass coaters, and under industry-friendly conditions (low preparation temperature, no substrate bias voltage). This is far from trivial: VO₂ is only one of many stoichiometries, VO₂(M1 \leftrightarrow R) is only one of many VO₂ polymorphs, and the preparation technique should include the possibility to shift T_{tr} to the room temperature (most often by doping of VO₂ by W) at preserved strength of the thermochromic transition. While our lab is involved in these efforts [33-35], the scope of the present paper is different.

Second, we need to maximize the quantified performance of thermochromic coatings in terms of integral luminous transmittance (T_{lum}) and modulation of integral solar energy transmittance (ΔT_{sol}). See Eqs. 1 and 2, respectively, where $T(\lambda, T_m)$ is a spectral transmittance at a measurement temperature T_m , $\varphi_{lum}(\lambda)$ is the luminous sensitivity of human eye and $\varphi_{sol}(\lambda)$ is the solar irradiance. If we let alone the trade-off between T_{lum} and ΔT_{sol} resulting from varied thickness of the thermochromic layer, there are ideas how to optimize both quantities in parallel. Examples include second-order antireflection layers [36], localized surface plasmon resonance in the high-temperature metallic state [37], or once again doping [38].

$$T_{lum} = \int_{380}^{780} \varphi_{lum}(\lambda) \varphi_{sol}(\lambda) T(\lambda, T_m) d\lambda / \int_{380}^{780} \varphi_{lum}(\lambda) \varphi_{sol}(\lambda) d\lambda \quad (1)$$

$$T_{sol} = \int_{300}^{2500} \varphi_{sol}(\lambda) T(\lambda, T_m) d\lambda / \int_{300}^{2500} \varphi_{sol}(\lambda) d\lambda \quad \text{and} \quad \Delta T_{sol} = T_{sol}(T_m < T_{tr}) - T_{sol}(T_m > T_{tr}) \quad (2)$$

The aim of the present work is to elaborate another idea, briefly mentioned in the review published by the author in 2022 [2]. It builds on the fact that the overall transmittance modulation includes not only the aforementioned well known strong modulation in the infrared but also much less investigated slight modulation in the visible. While the former is multiplied by only moderate solar irradiance when calculating ΔT_{sol} , the latter is multiplied by strong solar irradiance when calculating ΔT_{sol} . Because higher modulation of $T(\lambda, T_m)$ is multiplied by lower $\varphi_{sol}(\lambda)$ and vice versa, both these wavelength ranges can constitute comparable (in absolute value) contributions to the total ΔT_{sol} . Furthermore, while the contribution of the $T(\lambda, T_m)$ modulation in the infrared always has the desired sign (increasing ΔT_{sol}), the modulation of $T(\lambda, T_m)$ in the visible can have both signs (increasing [39-41] or decreasing [42-44] ΔT_{sol}). The impression given by the literature is that while couple of authors [39-41] achieved and published visible-range modulation of the desired sign and the resulting high ΔT_{sol} , these findings remain rather empirical than knowledge-based. Thus, there is an urgent need to investigate this phenomenon, constituting a large energy-saving potential.

A case can be made that the reason behind this phenomenon may be related to crystalline templates such as Cr_2O_3 [39] (it is not easy to be more specific without knowing the crystal orientation) and/or to the exact composition of $\text{VO}_{2\pm x}$ [2]. Thus, the present paper, far from exhausting this direction of research, is focused on (i) detailed presentation of the aforementioned phenomenon using our experimental data, and on (ii) using ab-initio calculations to clarify whether the modulation of $T(\lambda, T_m)$ in the visible can be significantly altered in the desired direction by lattice strain and/or slightly off-stoichiometric [O]/[V] ratio.

2. Methods

2.1 Experiment

The phenomenon studied is illustrated by detailed characteristics of two VO_2 coatings prepared in our lab [45,46] (papers which report their basic characteristics, but do not use and discuss them in the present context). One of these coatings (prepared on amorphous glass) exhibits negative transmittance modulation in the visible, while the other one (prepared on crystalline Si) exhibits positive modulation of measured extinction coefficient and calculated transmittance in the visible. Both coatings were prepared by reactive high-power impulse

magnetron sputtering (HiPIMS; ATC 2200-V AJA International Inc. system with a TruPlasma Highpulse 4002 Hüttinger Elektronik power supply) of V target in Ar+O₂ plasma. The substrates were at a floating potential. The duty cycle of the voltage pulses was 1% and the voltage pulse duration was 50 μ s (frequency 200 Hz; glass substrate) or 80 μ s (frequency 125 Hz; Si substrate). The deposition-averaged power density was around 13 Wcm⁻², the pulse-averaged power density was around 1.3 kWcm⁻² and the peak power density was 5 kWcm⁻². The Ar partial pressure was 1 Pa at a fixed Ar flow rate of 60 sccm. The specifics of this technique, delivering of high energy and momentum into the growing films by highly ionized fluxes of film-forming atoms, allowed us to prepare the coatings at a floating potential and a very low growth temperature of 250 °C (Si substrate) - 300 °C (glass substrate).

The elemental composition close to VO₂ was ensured by pulsed O₂ flow control: the flux of O₂ was not constant, but varied between 0 and 2 sccm by a logical controller which compares the actual and preset value of selected control quantity (in the present case O₂ partial pressure using a preset critical value of 15 mPa, in other cases target current). According to the phase analysis (Raman spectra and XRD patterns), the composition of at least the dominant crystalline (\Leftrightarrow potentially thermochromic) part of both samples is close to VO₂. The sample which does not exhibit the desired modulation in the visible may be slightly O-rich (there is a tiny peak of V₄O₉) [45]. The sample which does exhibit the desired modulation in the visible may be slightly V-rich (increasing $k(\lambda)$ in the infrared even for the semiconducting phase, shown also below) [46].

The optical constants $n(\lambda)$ and $k(\lambda)$ were measured by variable-angle spectroscopic ellipsometry using the J.A.Woollam VASE instrument equipped with the Instec heat/cool stage. The measurements were performed in reflection under angles 55, 60 and 65° (glass substrate) or 65, 70 and 75° (Si substrate), at temperatures $T_m = 25$ °C and 100 °C (safely below and above T_{tr} of undoped VO₂, respectively). The raw data were processed by an optical model implemented in the WVASE software and containing the substrate, VO₂ layer represented by a combination of one Cody-Lorentz oscillator with several Lorentz oscillators, and a surface roughness layer. The coating transmittance, resulting from measured (this subsection) or calculated (next subsection) optical constants, was calculated by the WVASE software which utilizes the transfer matrix formalism.

See our previous papers for further information such as time dependencies of voltage, current and O₂ partial pressure [33], energy-resolved mass spectroscopy [33], using deep oscillation magnetron sputtering instead of conventional HiPIMS [34], shift of T_{tr} toward the room temperature by doping [35], enhancement of T_{lum} and ΔT_{sol} by antireflection layers [36] or the effect of key process parameters on optical properties and electrical resistivity [33,45].

2.2 Modelling

The experimental data are complemented by ab-initio calculations utilizing Hubbard-corrected density-functional theory (DFT+ U [47]) as implemented in the Quantum Espresso (QE) package [48]. Note that the aim of these calculations is orthogonal to those reported for unstrained stoichiometric VO₂ previously [49-56]: neither to further develop the exceptionally challenging methodology of calculations of electronic structures of these strongly correlated materials, nor to reveal the effect of doping in the metal sublattice, but to provide information about possible effects of lattice strain and off-stoichiometric [O]/[V] ratio. The information which can be and is sought are not exact values of optical constants at exact λ , but whether it is realistically possible to achieve a quantitatively significant effect in the desired direction.

The technicalities shared by all steps of each calculation include expanding the valence electron wavefunction in a plane-wave basis set, treating of exchange and correlation effects using the PBE functional [57], Marzari-Vanderbilt smearing [58] of the occupations of electronic states around the Fermi level, and the U value for V 3d electrons in DFT+ U , employed to compensate the usual band gap underestimation of DFT, of 3.5 eV (following previously used 3.4 eV [53] - 3.5 eV [56]). The calculations were not spin polarized (no local magnetic moments were observed in VO₂(M1), see e.g. the discussion in [52]).

The calculation procedure at a given composition and given b/a (next paragraph) was the following. First, about ten different isotropic deformations have been applied, followed by relaxation of atomic positions and calculation of the total energy. Second, the lowest-energy volume has been identified by fitting the Birch equation of state, and the atomic positions have been relaxed also at this volume. In these first two steps the atom cores and inner electron shells were represented by ultrasoft Vanderbilt pseudopotentials [59], the wavefunction cutoff was 25 Ry, the k-point grid was 6×6×6 for the 12-atom cell and the smearing around the Fermi level was 0.5 eV. Third, the electronic structure has been recalculated using norm-conserving Troullier-Martins pseudopotentials [60], wavefunction cutoff of 60 Ry, k-point grid 12×12×12 for the 12-atom cell and smearing around the Fermi level of 0.1 eV. Fourth, the electronic structure has been used to calculate the dielectric tensor (spectral dependencies of real and imaginary part of the relative permittivity $\varepsilon_x(\lambda)$, $\varepsilon_y(\lambda)$ and $\varepsilon_z(\lambda)$) by the postprocessing code which is a part of the QE package. Fifth, the isotropic refractive index ($n(\lambda)$) and extinction coefficient ($k(\lambda)$) have been predicted by assuming equal volume fractions of crystals characterized by ε_x , ε_y and ε_z , and using Bruggemann effective medium approximation with a depolarization factor of 1/3. Sixth, transmittance has been calculated using the software VASE for 1 mm thick glass coated by (i) 50 nm thick layer of the investigated VO₂ and by (ii) state-of-the-art [36] three-layer coating combining 50 nm thick middle layer VO₂ with second-order antireflection layers made of 180 nm of ZrO₂ below and above it.

For each strain and each composition, the calculation has been performed for monoclinic VO₂(M1) (12-atom primitive cell characterized in the unstrained state by $b/a = 0.786523$, $c/a = 0.935922$ and $\cos\beta = -0.539447$) as well as for tetragonal VO₂(R) (6-atom primitive cell characterized in the unstrained state by $c/a = 0.626048$; may be converted to 12-atom cell resembling VO₂(M1) and characterized by $b/a = 0.798660$, $c/a = 0.942262$ and $\cos\beta = -0.530638$). The role of strain has been investigated by changing b/a from 90% to 110% of the preferred (unstrained) value at fixed c/a and $\cos\beta$ (the simplest out of many possibilities, but sufficient to fulfil the present aim), and the role of stoichiometry has been investigated by moving from 6-atom or 12-atom primitive cells to 48-atom supercells with up to 2 oxygen vacancies (the experimental data below indicate desired modulation in the visible in parallel to a relatively strong role of free charge carriers in the infrared, so understoichiometry in O has been considered more promising than overstoichiometry in O).

3. Results and discussion

The optical constants of both investigated polymorphs of VO₂ prepared on amorphous glass are shown in Fig. 1a. The best known consequence of the thermochromic transition from semiconductive VO₂(M1) to metallic VO₂(R) is significantly enhanced $k(\lambda)$ in the infrared. However, the information which is even more important for the present work is slightly lower $k(\lambda)$ of VO₂(R) in the UV range and in most of the visible range up to ≈ 645 nm (collectively

representing $\approx 70\%$ of solar energy in UV+VIS and $\approx 40\%$ of total solar energy). The optical constants of the same polymorphs of VO₂ prepared on crystalline Si are shown in Fig. 1b. While the overall qualitative impression is similar to that given by Fig. 1a, there is an important quantitative difference: $k(\lambda)$ of VO₂(R) is higher than that of VO₂(M1) not only in the infrared but also in whole visible range. It is also worth to point out the difference between both figures in terms of $k(\lambda)$ of VO₂(M1) in the infrared. In Fig. 1a this quantity decreases with λ , indicating negligible contribution of free charge carriers (negligible Drude term of permittivity), while in Fig. 1b this quantity increases with λ , indicating much stronger role of free charge carriers (arguably due to a slightly more metallic composition VO_{2-x}). How closely related is the latter observation to the desired sign of visible-range modulation is an important open question.

The spectral transmittance, calculated using the optical constants from Figs. 1a,b, is shown in Figs. 1c,d (the agreement of transmittance predicted using this methodology and measured transmittance has been confirmed previously [2]). Although the relationship between $k(\lambda)$ and $T(\lambda)$ is not straightforward (role of $n(\lambda)$ and of the interference), in the present case the trends are the same. The negative visible-range modulation of $k(\lambda)$ in Fig. 1a is largely responsible for the negative visible-range modulation of $T(\lambda)$ in Fig. 1c, while the positive visible-range modulation of $k(\lambda)$ in Fig. 1b is largely responsible for the positive visible-range modulation of $T(\lambda)$ in Fig. 1d. These trends are valid for both coating designs considered: VO₂(50 nm) layers on glass as well as ZrO₂(180 nm) - VO₂(50 nm) - ZrO₂(180 nm) trilayers on glass. The figure also indicates, beyond the scope of the present paper, the advantage of second-order antireflection layers (180 nm of ZrO₂ with $n_{550} = 2.15$; figure S1 in the Supplementary material) in terms of not only T_{lum} but also ΔT_{sol} . Second-order maxima in the visible lead to first-order maxima at approximately $3\times$ longer λ in the infrared, and the enhanced $T(\lambda)$ values in the infrared lead to enhanced $T(\lambda)$ modulation in the infrared [36].

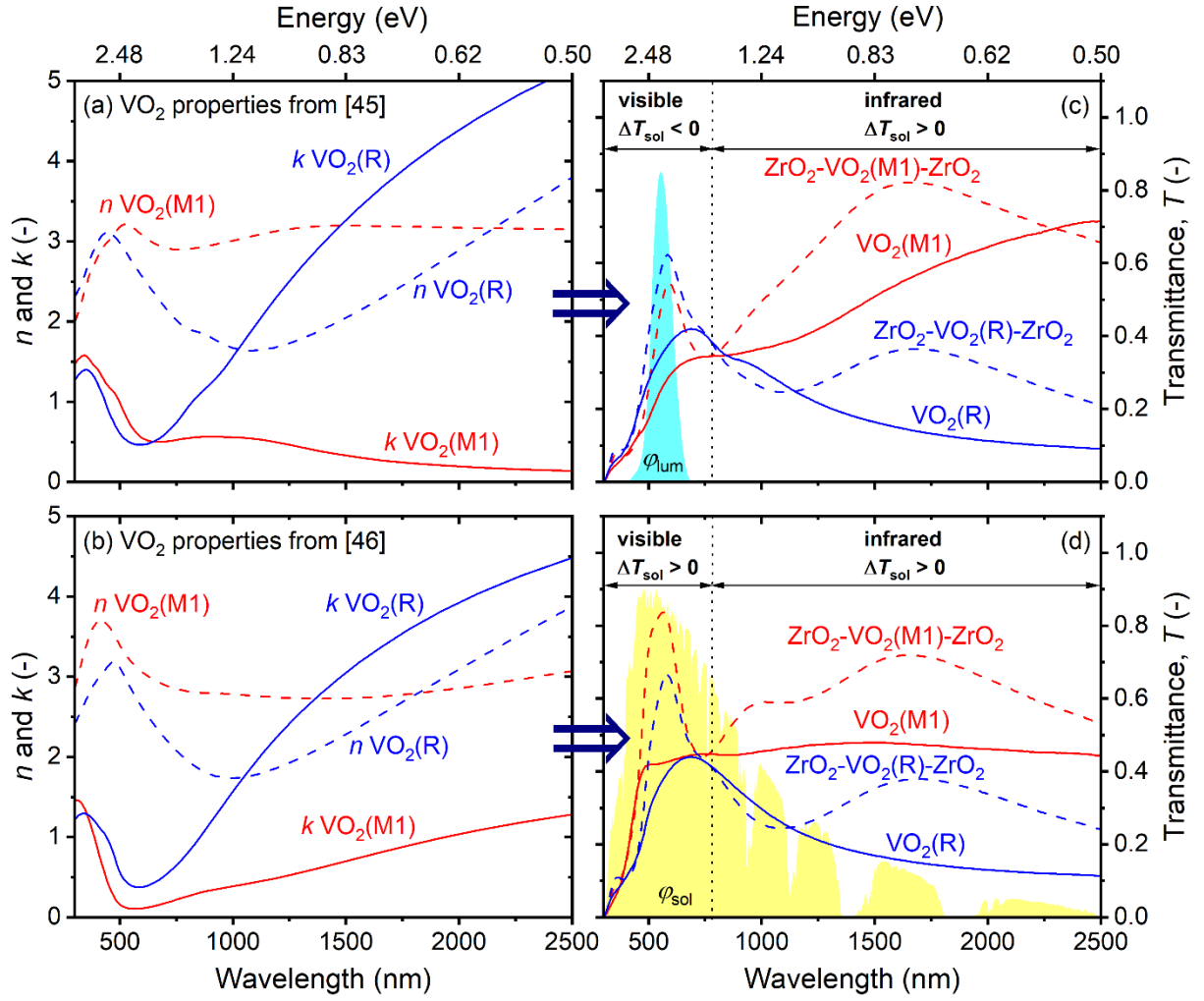


Figure 1: Measured refractive index, n , of VO_2 (dashed lines in panels a[45] and b[46]), measured extinction coefficient, k , of VO_2 (full lines in panels a[45] and b[46]), calculated transmittance, T , of $\text{VO}_2(50 \text{ nm})$ on glass (full lines in panels c,d) and calculated transmittance of $\text{ZrO}_2(180 \text{ nm}) - \text{VO}_2(50 \text{ nm}) - \text{ZrO}_2(180 \text{ nm})$ trilayers on glass (dashed lines in panels c,d). Red lines are for the low-temperature semiconductive polymorph $\text{VO}_2(\text{M1})$ and blue lines are for the high-temperature metallic polymorph $\text{VO}_2(\text{R})$. The shaded areas in panels c and d (arbitrary units without any vertical axis) correspond to the luminous sensitivity of human eye ϕ_{lum} and spectral solar irradiance ϕ_{sol} , respectively. Note the qualitative difference between visible-range modulation of $k(\lambda)$ in panels a,c (leading to opposite signs of the integral contributions of visible-range and infrared-range wavelengths to ΔT_{sol} ; amorphous glass template) and in panels b,d (the same signs of both contributions; crystalline Si template).

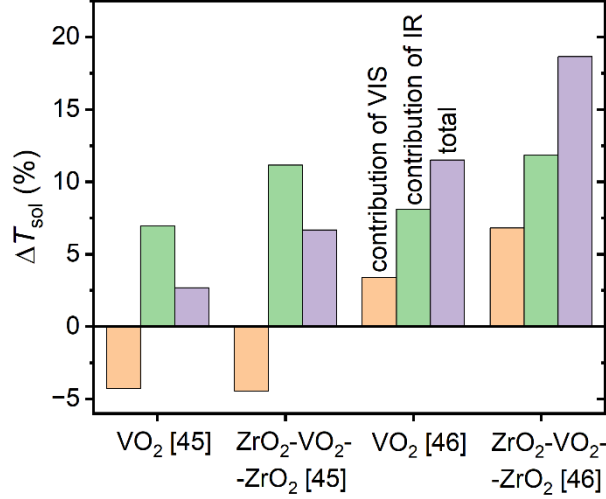


Figure 2: Calculated contribution of visible-range light (orange columns) and infrared light (green columns) to the total modulation of integral solar energy transmittance, ΔT_{sol} (violet columns) for VO₂(50 nm) on glass and ZrO₂(180 nm) - VO₂(50 nm) - ZrO₂(180 nm) trilayers on glass. The measured VO₂ properties used to calculate ΔT_{sol} correspond to Fig. 1a (first and second set of columns) and Fig. 1b (third and fourth set of columns).

The qualitative impression given by Fig. 1 is quantified in Fig. 2. The measure of energy saving, ΔT_{sol} , is shown using triplets of columns: contribution of predominantly visible wavelengths from 300 to 780 nm (the importance of near UV is limited by transmittance of the glass substrate), contribution of infrared wavelengths from 780 to 2500 nm, and the total ΔT_{sol} value given by the sum of the previous two. On the one hand, in the case of VO₂ properties shown in Fig. 1a, the beneficial positive modulation in the infrared is to a large extent wasted because of the negative modulation in the visible: $\Delta T_{\text{sol}} = -4.3\%$ (VIS) + 7.0% (IR) = 2.7% for VO₂(50 nm), and $\Delta T_{\text{sol}} = -4.5\%$ (VIS) + 11.2% (IR) = 6.7% for ZrO₂(180 nm) - VO₂(50 nm) - ZrO₂(180 nm). On the other hand, in the case of VO₂ properties shown in Fig. 1b, the beneficial positive modulation in the infrared is supported by also positive modulation in the visible: $\Delta T_{\text{sol}} = 3.4\%$ (VIS) + 8.1% (IR) = 11.5% for VO₂(50 nm), and $\Delta T_{\text{sol}} = 6.8\%$ (VIS) + 11.9% (IR) = 18.7% for ZrO₂(180 nm) - VO₂(50 nm) - ZrO₂(180 nm).

Indeed, the integral transmittances once again confirm that the dramatical differences resulting from considering VO₂ properties from different sources take place only in the visible. It is also worth to add that the advantage of visible-range modulation of VO₂ properties obtained in [46] is given not only by its direct consequences (positive contribution of VIS to ΔT_{sol} in the third set of columns in Fig. 2), but also by the possibility to tailor the second-order antireflection layer in that way that its functionality is higher in the low-temperature state of the coating (2× higher contribution of VIS to ΔT_{sol} in the fourth than in the third set of columns in Fig. 2). On the contrary, the role of infrared wavelengths is almost independent of the source of VO₂ properties, for VO₂(50 nm) (contribution of IR to ΔT_{sol} in the first and third set of columns in Fig. 2 of ≈7-8%) as well as for ZrO₂(180 nm) - VO₂(50 nm) - ZrO₂(180 nm) (contribution of IR to ΔT_{sol} in the second and fourth set of columns in Fig. 2 of ≈11-12%, enhanced by the aforementioned first-order interference maximum in the infrared).

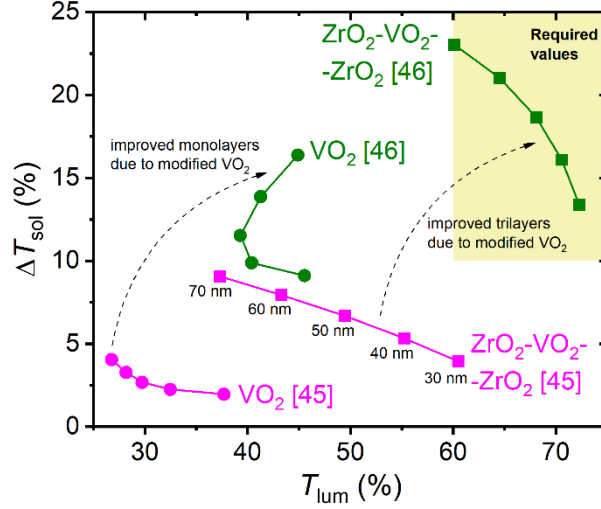


Figure 3: Calculated average luminous transmittance, T_{lum} , and modulation of integral solar energy transmittance, ΔT_{sol} , for VO_2 monolayers on glass (balls) and $ZrO_2(180\text{ nm}) - VO_2 - ZrO_2(180\text{ nm})$ trilayers on glass (squares). The data are shown for VO_2 properties corresponding to Fig. 1a (magenta) and Fig. 1b (green), and for VO_2 thicknesses of 30 nm to 70 nm with a step of 10 nm. The shaded area represents the required T_{lum} and ΔT_{sol} values for smart-window applications.

The whole calculated thermochromic performance in terms of not only ΔT_{sol} but also T_{lum} (averaged over the low- and high-temperature state) can be seen in Fig. 3. The performance is shown not only for the VO_2 thickness of 50 nm which is used throughout this paper, but also for other thicknesses from 30 to 70 nm. One of the roles of this figure is to avoid any impression that the altered modulation in the visible can improve ΔT_{sol} only at a cost of worse T_{lum} . In the present case where altered modulation means in the first place lowered visible-range $k(\lambda)$ of $VO_2(M1)$ rather than e.g. enhanced visible-range $k(\lambda)$ of $VO_2(R)$, the figure clearly shows that the transition from VO_2 properties in Fig. 1a to those in Fig. 1b improves both T_{lum} and ΔT_{sol} . This is not to be confused with the trade-off between T_{lum} and ΔT_{sol} resulting from varied VO_2 thickness, exhibited by all dependencies in Fig. 3 (except that T_{lum} of the more transparent VO_2 monolayer exhibits a non-monotonic dependence on the thickness of this monolayer because of the interference on it). Note that as long as the altered modulation in the visible shifts the whole thickness dependence in the desired top right direction, this trade-off would allow one to change the thickness and improve ΔT_{sol} at preserved T_{lum} even if the modulation was achieved by enhanced visible-range $k(\lambda)$. The improved properties of $ZrO_2(180\text{ nm}) - VO_2 - ZrO_2(180\text{ nm})$ trilayer fulfil the frequent requirement ([2] and Refs. therein) for cost-effective smart-window applications: $T_{lum} \geq 60\%$ and $\Delta T_{sol} \geq 10\%$.

The calculated spectral dependencies of optical constants of both unstrained and strained VO_2 are shown in Figs. 4a,b. Although the aforementioned aim is to capture the qualitative effect of strain rather than to predict exact $n(\lambda)$ and $k(\lambda)$, the figures actually reproduce many of the features observed (Fig. 1) in the same wavelength range experimentally. There is (i) $n(\lambda)$ of $VO_2(M1)$ of around 3, (ii) drop of minimum values of $n(\lambda)$ after the transition to $VO_2(R)$, (iii) $k(\lambda)$ of $VO_2(M1)$ ranging from low values in IR to 1.5-2.0 in VIS and near UV and, above all (iv) the main merit of thermochromic VO_2 : steep increase of $k(\lambda)$ in IR after the transition to $VO_2(R)$. The biggest quantitative difference from Fig. 1 is overestimated $k(\lambda)$ of $VO_2(M1)$ in the central part of the presented range: reason why Figs. 4c and 5c show ratios rather than

values of transmittances. For the comparison of modelling and experiment note also figures S2 and S3 in the Supplementary material.

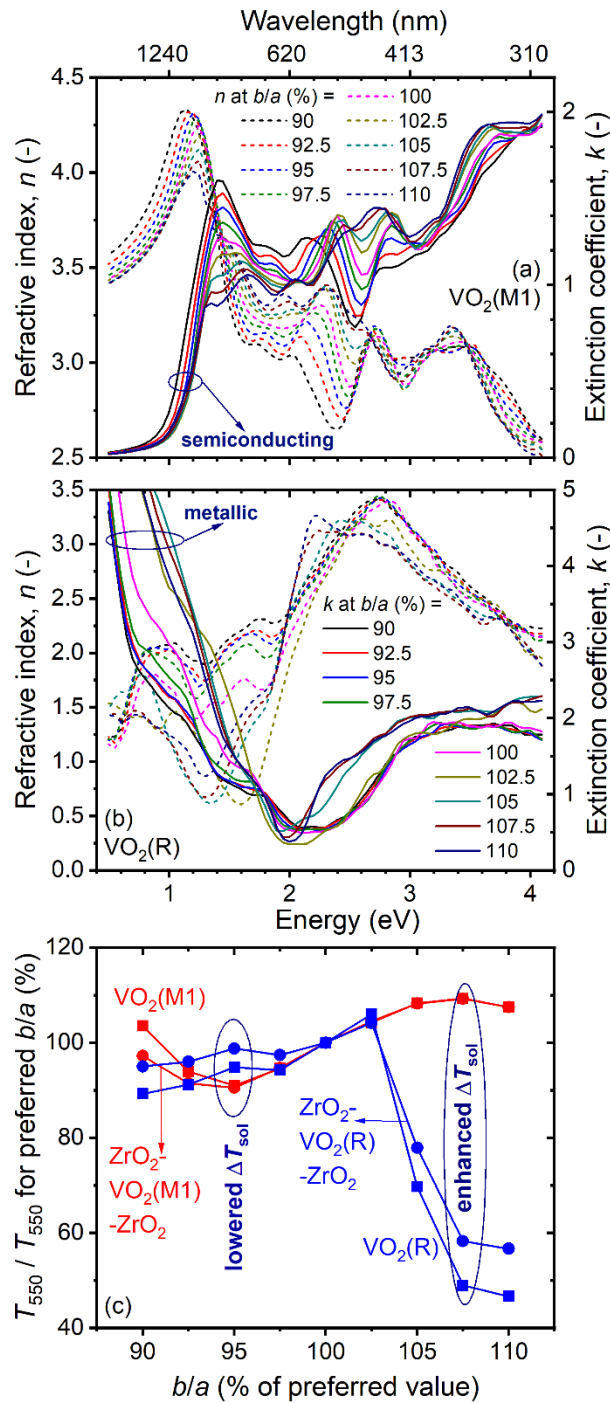


Figure 4: Effect of varied lattice constant ratio b/a on calculated refractive index (dashed lines) and extinction coefficient (solid lines) of VO₂(M1) (panel a) and VO₂(R) (panel b). Panel c shows the transmittance at 550 nm, T_{550} , calculated using this n and k of both polymorphs for VO₂(50 nm) on glass (squares) and ZrO₂(180 nm) - VO₂(50 nm) - ZrO₂(180 nm) trilayers on glass (circles) and shown as a ratio to T_{550} calculated for preferred b/a .

Figures 4a,b show that on the one hand, the strain-induced changes preserve the main qualitative feature of the thermochromic transition from VO₂(M1) to VO₂(R): increase of $k(\lambda)$

at all wavelengths above $\approx 800 \pm 100$ nm (limit decreasing with b/a), i.e. all energies below $\approx 1.55 \pm 0.20$ eV (limit increasing with b/a). On the other hand, there are complicated strain-induced changes of both $n(\lambda)$ and $k(\lambda)$ in the visible, including different signs of these changes at different wavelengths for the same strain. To put an example for 550 nm = 2.25 eV (middle of the visible range and close to the maximum of $\varphi_{\text{sol}}(\lambda)$), increasing b/a of VO₂(M1) leads to monotonically increasing n_{550} at mostly decreasing k_{550} , and increasing b/a of VO₂(R) leads to a convex dependence of both n_{550} and k_{550} , at particularly steep increase of k_{550} at b/a enhanced to 105-110% of the preferred value. Although a case can be made that (despite using DFT+ U instead of just DFT) 550 nm in simulations does not exactly correspond to 550 nm in the experiment, (i) this is consistent with the aforementioned aim of the present calculations, and (ii) the most significant effect, increase of $k(\lambda)$ of VO₂(R) at enhanced b/a , is actually observable in Fig. 4b not only at 550 nm but in a wide range of wavelengths.

The presented strain-induced changes of optical constants of both VO₂(M1) and VO₂(R) directly lead to strain-induced changes of their transmittance. This is shown in Fig. 4c for the same two coating designs as in Figs. 1-3, for brevity only at the aforementioned $\lambda = 550$ nm = 2.25 eV. The figure confirms the intuition that the effect of lattice strain of VO₂ on individual contributions to ΔT_{sol} may be positive as well as negative. To put a specific example, the effect on the modulation of T_{550} is positive at b/a enhanced to at least 105% and negative at b/a lowered to about 95% of the preferred value, independently of the coating design (VO₂(50 nm) or ZrO₂(180 nm) - VO₂(50 nm) - ZrO₂(180 nm)). Quantitatively, the strain-induced changes of T_{550} of both polymorphs at b/a up to 105% are within approximately $\pm 10\%$, and the changes at $b/a = 105$ -110% are even much more significant. The importance of the "small" changes on the order of 10% is emphasized by their comparison with experimental visible-range contributions to ΔT_{sol} in Fig. 2, which are on the same order. On the minus side, the positive effect at such enhanced b/a is mostly due to enhanced k_{550} and in turn lowered T_{550} of VO₂(R) and only slightly due to enhanced T_{550} of VO₂(M1), indicating that the present example of a strain tensor does not constitute the most promising one. It is perfectly likely that other strain tensors used in the future may be even more beneficial and/or easier to realize (intentionally or by chance) using specific crystalline substrates. One reason why the available information is still very limited is rarely reported preferred crystal orientation (partially resulting from the preference of grazing-incidence XRD over Bragg-Brentano XRD in the case of very thin VO₂ layers).

The calculated spectral dependencies of optical constant of both VO₂ and vacancy-containing VO_{2-x} are shown in Figs. 5a,b. There is a significant qualitative difference between the effect of strain in Figs. 4a,b and the effect of stoichiometry in Figs. 5a,b. While the effect of strain is significant in the visible but does not affect the order of magnitude of low $k(\lambda)$ of VO₂(M1) and high $k(\lambda)$ of VO₂(R) in the infrared, the effect of oxygen vacancies is the largest in terms of $k(\lambda)$ of VO₂(M1) in the infrared.

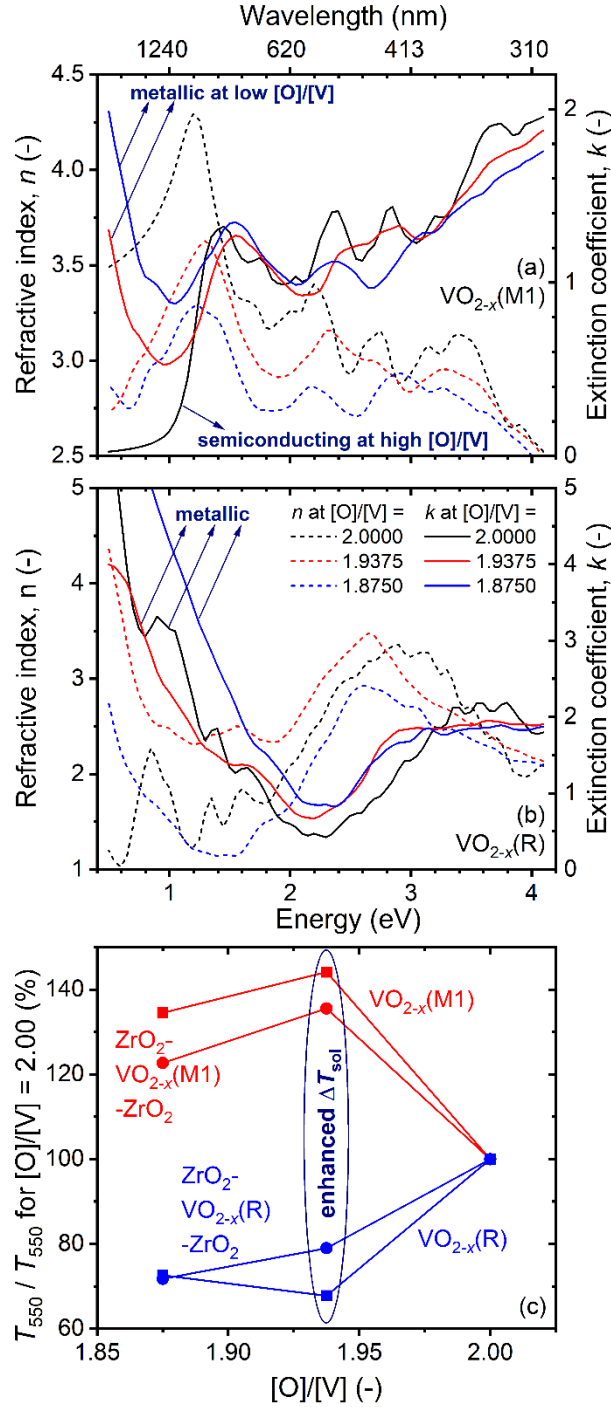


Figure 5: Effect of varied composition on calculated refractive index (dashed lines) and extinction coefficient (solid lines) of $\text{VO}_{2-x}(\text{M1})$ (panel a) and $\text{VO}_{2-x}(\text{R})$ (panel b). Panel c shows the transmittance at 550 nm, T_{550} , calculated using this n and k of both polymorphs for $\text{VO}_2(50 \text{ nm})$ on glass (squares) and $\text{ZrO}_2(180 \text{ nm}) - \text{VO}_2(50 \text{ nm}) - \text{ZrO}_2(180 \text{ nm})$ trilayers on glass (circles) and shown as a ratio to T_{550} calculated for stoichiometric VO_2 .

First, $\text{VO}_2(\text{M1})$ ($\text{V}_{16}\text{O}_{32}$ simulation cell) once again exhibits, in agreement with the experiment, dispersion characteristic of a semiconductor: decreasing $k(\lambda)$ in the infrared with decreasing energy, at no role of free charge carriers. Second, $\text{VO}_{1.9375}(\text{M1})$ ($\text{V}_{16}\text{O}_{31}$ simulation cell), exhibits the opposite: increasing $k(\lambda)$ in the infrared (below $\approx 1 \text{ eV}$) with decreasing energy, i.e. a usual fingerprint of free charge carriers. In other words, one vacancy per 32 O

positions (concentration chosen due to computational costs) is sufficient for a significant Drude term of permittivity, and even lower vacancy concentrations may be thus recommended for future experimental efforts. This is consistent with the fact that $\text{VO}_{1.9375} = \text{V}_{16}\text{O}_{31}$ is actually as far as halfway between VO_2 and the next phase in the V-O phase diagram, V_8O_{15} . Third, $\text{VO}_{1.8750}(\text{M1})$ ($\text{V}_{16}\text{O}_{30}$ simulation cell) confirms this trend: $2\times$ higher vacancy concentration further increases (albeit less than $2\times$) $k(\lambda)$ in the infrared. On the contrary, the corresponding effect of O vacancies on $\text{VO}_{2-x}(\text{R})$ is much weaker: this phase is metallic for all compositions investigated, and its $k(\lambda)$ in the infrared is consequently (i) increasing with decreasing energy and (ii) still higher than that of $\text{VO}_{2-x}(\text{M1})$ (note different vertical scales) regardless the number of vacancies. To put an example of the predicted effect on infrared transmittance, the presence of 1-2 vacancies decreases the transmittance of 50 nm thick $\text{VO}_2(\text{M1})$ at $\lambda = 2500$ nm from 70% to 36-48% and its modulation after the transition to $\text{VO}_2(\text{R})$ from 58% to 33-36%.

The effect of vacancies in the visible shown in Figs. 5a,b is much weaker than that in the infrared, and it is (in the present compositional and strain range) on the same order as the effect of lattice strain in the visible shown in Figs. 4a,b. However, this effect is important also here, and for the same reason: multiplication by high $\varphi_{\text{sol}}(\lambda)$. If we follow the previous figure and once again put an example for 550 nm = 2.25 eV, it is interesting that the effect of the creation of vacancies is in the same direction as that of the enhanced b/a : lower k_{550} of $\text{VO}_{2-x}(\text{M1})$ and higher k_{550} (increase which is once again observable in a wide range of wavelengths) of $\text{VO}_{2-x}(\text{R})$.

Again, the presented composition-dependent changes of optical constants of both $\text{VO}_2(\text{M1})$ and $\text{VO}_2(\text{R})$ directly lead to composition-dependent changes of their transmittance shown in Fig. 5c. We can observe a different way (incorporation of vacancies instead of increasing b/a) how to achieve the desired effect on the modulation of T_{550} and in turn the enhanced energy saving in terms of ΔT_{sol} . Furthermore, contrary to the role of b/a , the desired effect is this time achieved not only by lower T_{550} of $\text{VO}_2(\text{R})$ (improving ΔT_{sol} at a cost of T_{lum}) but equally importantly also by higher T_{550} of $\text{VO}_2(\text{M1})$ (improving both ΔT_{sol} and T_{lum} simultaneously).

Thus, the data in Fig. 5 indicate that manipulating the exact composition is equally promising way of achieving the desired visible-range contribution to ΔT_{sol} as manipulating the lattice deformation. A case can be made that manipulating the composition is even more promising because it can be utilized on any growth template (e.g., any material of antireflection layer below the active thermochromic layer). A synergy of both these options is worth a consideration as well, including the possibility that the former (creation of vacancies) may be induced by the latter (template-dependent lattice strain). This constitutes one possible explanation of the difference between the two samples prepared in a similar way and presented in Fig. 1: no observable role of free charge carriers and harmful modulation in the visible on the amorphous template, fingerprint of free charge carriers and desired modulation in the visible on the crystalline template.

4. Conclusions

Modulation of integral solar energy transmittance, ΔT_{sol} , constitutes a measure of energy saving using VO_2 -based thermochromic coatings. Contributions of visible and infrared range to ΔT_{sol} can have comparable absolute values. While the contribution of infrared range to ΔT_{sol} always has the desired sign, the contribution of visible range to ΔT_{sol} can have both signs. This

has been observed even for VO₂ layers prepared using very similar deposition protocols except different growth templates.

Ab-initio calculations reveal that the modulation in the visible can be affected by lattice strain as well as by slight changes of the VO_{2±x} stoichiometry. For example, desired direction and significant size of this effect has been achieved by increasing b/a to $\geq 105\%$ of the preferred value, or alternatively by introducing 1-2 O vacancies per 32 O positions. The latter also increases the metallicity of the low-temperature phase VO₂(M1), which is relevant for the explanation of the presented experimental data as well.

Collectively, the results show that the efficiency of energy-saving thermochromic VO₂ can be significantly enhanced (ΔT_{sol} in the presented example from 2.7% to 11.5% or from 6.7% to 18.7% depending on the coating design) by slight changes of its properties in the visible. In order to fully utilize this potential and to avoid the opposite, further experimental as well as theoretical research is needed. On the experimental side this may require investigation of preferred crystal orientation in general and epitaxial growth on various templates in particular, as well as precise compositional measurements. Antireflection layers below VO₂ can simultaneously fulfil also the role of crystalline growth template and induce the lattice strain. On the theoretical side this may require extensive calculations considering various strain tensors or even lower vacancy concentrations, as well as further improvement of the exactness of these calculations for strongly correlated VO₂. Focus on a combination of both effects (compositional changes induced by a lattice strain) may be relevant on both sides.

Data availability

Data will be made available on request.

Acknowledgment

This work was supported by the project Quantum materials for applications in sustainable technologies (QM4ST), funded as project No. CZ.02.01.01/00/22_008/0004572 by Programme Johannes Amos Comenius, call Excellent Research. Computational resources were provided by the e-INFRA CZ project (ID:90254), supported by the Ministry of Education, Youth and Sports of the Czech Republic.

References

- 1 F.J. Morin, Oxides which show a metal-to-insulator transition at the Neel temperature, *Phys. Rev. Lett.* 3 (1959) 34-36.
- 2 J. Houska, Design and reactive magnetron sputtering of thermochromic coatings, *J. Appl. Phys.* 131 (2022) 110901.
- 3 M. Aburas, V. Soebarto, T. Williamson, R. Liang, H. Ebendorff-Heidepriem, Y. Wuc, Thermochromic smart window technologies for building application: A review, *Appl. Energ.* 255 (2019) 113522.
- 4 K. Liu, S. Lee, S. Yang, O. Delaire, J. Wu, Recent progresses on physics and applications of vanadium dioxide, *Materials Today* 21 (2018) 875-896.
- 5 R. Shi, N. Shen, J. Wang, W. Wang, A. Amini, N. Wang, C. Cheng, Recent advances in fabrication strategies, phase transition modulation, and advanced applications of vanadium dioxide, *Appl. Phys. Rev.* 6 (2019) 011312.

- 6 Y. Zhang, W. Xiong, W. Chen, Y. Zheng, Recent progress on vanadium dioxide nanostructures and devices: fabrication, properties, applications and perspectives, *Nanomaterials* 11 (2021) 338.
- 7 T.D. Vu, Z. Chen, X. Zeng, M. Jiang, S. Liu, Y. Gao, Y. Long, Physical vapour deposition of vanadium dioxide for thermochromic smart window applications, *J. Mater. Chem. C* 7, (2019) 2121-2145.
- 8 X. Cao, T. Chang, Z. Shao, F. Xu, H. Luo, P. Jin, Challenges and opportunities toward real application of VO₂-based smart glazing, *Matter* 2 (2020) 862-881.
- 9 N.R. Mlyuka, G.A. Niklasson, C.G. Granqvist, Thermochromic VO₂-based multilayer films with enhanced luminous transmittance and solar modulation, *Phys. Stat. Sol. A* 206 (2009) 2155-2160.
- 10 A. Lafort, H. Kebaili, S. Goumri-Said, O. Deparis, R. Cloots, J. De Coninck, M. Voué, F. Mirabella, F. Maseri, S. Lucas, Optical properties of thermochromic VO₂ thin films on stainless steel: experimental and theoretical studies, *Thin Solid Films* 519 (2011) 3283-3287.
- 11 Q. Ya, C. Jie, L. Yuan, Y. Xing, Y. Hua, X. Kai, Fabrication of low phase transition temperature vanadium oxide films by direct current reactive magnetron sputtering and oxidation post-anneal method, *Infrared Phys. Technol.* 67 (2014) 126-130.
- 12 D.-P. Zhang, M.-D. Zhu, Y. Liu, K. Yang, G.-X. Liang, Z.-H. Zheng, X.-M. Cai, P. Fan, High performance VO₂ thin films growth by DC magnetron sputtering at low temperature for smart energy efficient window application, *J. Alloy. Compd.* 659 (2016) 198-202.
- 13 G. Sun, X. Cao, X. Li, S. Bao, N. Li, M. Liang, A. Gloter, H. Gu, P. Jin, Low-temperature deposition of VO₂ films with high crystalline degree by embedding multilayered structure, *Sol. Energy Mater. Sol. Cells* 161 (2017) 70-76.
- 14 T. Chang, X. Cao, N. Li, S. Long, X. Gao, L.R. Dedon, G. Sun, H. Luo, P. Jin, Facile and low-temperature fabrication of thermochromic Cr₂O₃/VO₂ smart coatings: enhanced solar modulation ability, high luminous transmittance and uv-shielding function, *ACS Appl. Mater. Interfaces* 9 (2017) 26029-26037.
- 15 C. Ji, Z. Wu, L. Lu, X. Wu, J. Wang, X. Liu, H. Zhou, Z. Huang, J. Gou, Y. Jiang, High thermochromic performance of Fe/Mg co-doped VO₂ thin films for smart window applications, *J. Mater. Chem. C* 6 (2018) 6502.
- 16 L. Lu, Z. Wu, C. Ji, M. Song, H. Feng, X. Ma, Y. Jiang, Effect of Fe doping on thermochromic properties of VO₂ films, *J. Mater. Sci. Mater. Electron.* 29 (2018) 5501-5508.
- 17 Y. Shigesato, M. Enomoto, H. Odaka, Thermochromic VO₂ films deposited by RF magnetron sputtering using V₂O₃ or V₂O₅ targets, *Jpn. J. Appl. Phys.* 39 (2000) 6016-6024.
- 18 G. Xu, P. Jin, M. Tazawa, K. Yoshimura, Optimization of antireflection coating for VO₂-based energy efficient window, *Sol. Energy Mater. Sol. Cells* 83 (2004) 29-37.
- 19 D. Brassard, S. Fourmaux, M. Jean-Jacques, J. C. Kieffer, M.A. El Khakani, Grain size effect on the semiconductor-metal phase transition characteristics of magnetron-sputtered VO₂ thin films, *Appl. Phys. Lett.* 87 (2005) 051910.
- 20 A. Romanyuk, R. Steiner, L. Marot, P. Oelhafen, Temperature-induced metal-semiconductor transition in W-doped VO₂ films studied by photoelectron spectroscopy, *Sol. Energy Mater. Sol. Cells* 91 (2007) 1831-1835.
- 21 H. Kakiuchida, P. Jin, M. Tazawa, Control of thermochromic spectrum in vanadium dioxide by amorphous silicon suboxide layer, *Sol. Energy Mater. Sol. Cells* 92 (2008) 1279-1284.
- 22 H. Koo, H.W. You, K.E. Ko, O.-J. Kwon, S.H. Chang, C. Park, Thermochromic properties of VO₂ thin film on SiN_x buffered glass substrate, *Appl. Surf. Sci.* 277 (2013) 237-241.
- 23 Y. Xiong, Q.-Y. Wen, Z. Chen, W. Tian, T.-L. Wen, Y.-L. Jing, Q.-H. Yang, H.-W. Zhang, Tuning the phase transitions of VO₂ thin films on silicon substrates using ultrathin Al₂O₃ as buffer layers, *J. Phys. D Appl. Phys.* 47 (2014) 455304.

- 24 N.H. Azhan, K. Su, K. Okimura, J. Sakai, Radio frequency substrate biasing effects on the insulator-metal transition behavior of reactively sputtered VO₂ films on sapphire (001), *J. Appl. Phys.* 117 (2015) 185307.
- 25 M.K. Dietrich, F. Kuhl, A. Polity, P.J. Klar, Optimizing thermochromic VO₂ by co-doping with W and Sr for smart window applications, *Appl. Phys. Lett.* 110 (2017) 141907.
- 26 Y. Yang, Y. Yao, B. Zhang, H. Lin, Z. Luo, C. Gao, C. Zhang, C. Kang, Investigating metal–insulator transition and structural phase transformation in the (010)-VO₂/(001)-YSZ epitaxial thin films, *Materials* 11 (2018) 1713.
- 27 H.C. Ho, Y.C. Lai, K. Chen, T.D. Dao, C.H. Hsueh, T. Nagao, High quality thermochromic VO₂ films prepared by magnetron sputtering using V₂O₅ target with in situ annealing, *Appl. Surf. Sci.* 495 (2019) 143436.
- 28 J.-P. Fortier, B. Baloukas, O. Zabeida, J.E. Klemberg-Sapieha, L. Martinu, Thermochromic VO₂ thin films deposited by HiPIMS, *Sol. Energy Mater. Sol. Cells* 125 (2014) 291-296.
- 29 Aijaz, Y.-X. Ji, J. Montero, G.A. Niklasson, C.G. Granqvist, T. Kubart, Low-temperature synthesis of thermochromic vanadium dioxide thin films by reactive high power impulse magnetron sputtering, *Sol. Energy Mater. Sol. Cells* 149 (2016) 137-144.
- 30 B. Baloukas, S. Loquai, L. Martinu, VO₂-based thermally active low emissivity coatings, *Sol. Energy Mater. Sol. Cells* 183 (2018) 25-33.
- 31 J.L. Victor, C. Marcel, L. Sauques, N. Penin, A. Rougier, High quality thermochromic VO₂ thin films deposited at room temperature by balanced and unbalanced HiPIMS, *Sol. Energy Mater. Sol. Cells* 227 (2021) 111113.
- 32 Y. Choi, Y. Jung, H. Kim, Low-temperature deposition of thermochromic VO₂ thin films on glass substrates, *Thin Solid Films* 615 (2016) 437-445.
- 33 J. Vlček, D. Kolenatý, J. Houška, T. Kozák, R. Čerstvý, Controlled reactive HiPIMS-effective technique for low-temperature (300 °C) synthesis of VO₂ films with semiconductor-to-metal transition, *J. Phys. D: Appl. Phys.* 50 (2017) 38LT01.
- 34 J. Vlček, M. Kaufman, A.D. Pajdarová, S. Haviar, R. Čerstvý, J. Houška, M. Farahani, Detailed pathway for a fast low-temperature synthesis of strongly thermochromic W-doped VO₂ films with a low transition temperature, *J. Phys. D Appl. Phys.* 56 (2023) 505301.
- 35 M. Kaufman, J. Vlcek, J. Houska, R. Cerstvy, S. Farrukh, M. Chargaoui, S. Haviar, J.C. Jiang, E.I. Meletis, S. Kos, High-Performance Thermochromic YSZ/V_{0.986}W_{0.014}O₂/YSZ Coatings for Energy-Saving Smart Windows, *Sol. Energy Mater. Sol. Cells* 263 (2023) 112570.
- 36 J. Houska, D. Kolenaty, J. Vlcek, T. Barta, J. Rezek, R. Cerstvy, Significant improvement of the performance of ZrO₂/V_{1-x}W_xO₂/ZrO₂ thermochromic coatings by utilizing a second-order interference, *Sol. Energy Mater. Sol. Cells* 191 (2019) 365-371.
- 37 C.G. Granqvist, G.A. Niklasson, Thermochromic oxide-based thin films and nanoparticle composites for energy-efficient glazings, *Buildings* 7 (2017) 3.
- 38 M.K. Dietrich, B.G. Kramm, M. Becker, B.K. Meyer, A. Polity, P.J. Klar, Influence of doping with alkaline earth metals on the optical properties of thermochromic VO₂, *J. Appl. Phys.* 117 (2015) 185301.
- 39 T. Chang, X. Cao, L.R. Dedon, S. Long, A. Huang, Z. Shao, N. Li, H. Luo, P. Jin, Optical design and stability study for ultrahigh-performance and long-lived vanadium dioxide-based thermochromic coatings, *Nano Energy* 44 (2018) 256-264.
- 40 Y. Zhang, B. Li, Z. Wang, S. Tian, B. Liu, X. Zhao, N. Li, G. Sankar, S. Wang, Facile preparation of Zn₂V₂O₇-VO₂ composite films with enhanced thermochromic properties for smart windows, *ACS Appl. Electron. Mater.* 3 (2021) 2224-2232.
- 41 Z. Chen, Y. Tang, A. Ji, L. Zhang, Y. Gao, Large-scale preparation of durable VO₂ nanocomposite coatings, *ACS Appl. Nano Mater.* 4 (2021) 4048-4054.

- 42 S. Loquai, B. Baloukas, J.E. Klemberg-Sapieha, L. Martinu, HiPIMS-deposited thermochromic VO₂ films with high environmental stability, *Sol. Energy Mater. Sol. Cells* 160 (2017) 217–224.
- 43 E. Gagaoudakis, E. Aperathitis, G. Michail, G. Kiriakidis, V. Binas, Sputtered VO₂ coatings on commercial glass substrates for smart glazing applications, *Sol. Energy Mater. Sol. Cells* 220 (2021) 110845.
- 44 H. Zong, S. Zhang, L. Bian, H. Chen, Z. Liu, B. Sun, W. Qiao, L. Yan, Q. Hu, M. Li, Preparation and characterization of VO₂/Cu-Zr NPs/VO₂ composite films with enhanced thermochromic properties, *J. Alloys Compd.* 967 (2023) 171654.
- 45 J. Houska, D. Kolenaty, J. Vlcek, R. Cerstvy, Properties of thermochromic VO₂ films prepared by HiPIMS onto unbiased amorphous glass substrates at a low temperature of 300 °C, *Thin Solid Films* 660 (2018) 463-470.
- 46 J. Houska, D. Kolenaty, J. Rezek, J. Vlcek, Characterization of thermochromic VO₂ (prepared at 250° C) in a wide temperature range by spectroscopic ellipsometry, *Appl. Surf. Sci.* 421 (2017) 529-534.
- 47 V. I. Anisimov, F. Aryasetiawan, A. I. Lichtenstein, First-principles calculations of the electronic structure and spectra of strongly correlated systems: the LDA+U method, *J. Phys.: Condens. Matter* 9 (1997) 767-808.
- 48 P. Giannozzi, O. Andreussi, T. Brumme, O. Bunau, M. Buongiorno Nardelli, M. Calandra, R. Car, C. Cavazzoni, D. Ceresoli, M. Cococcioni, N. Colonna, I. Carnimeo, A. Dal Corso, S. de Gironcoli, P. Delugas, R. A. DiStasio Jr, A. Ferretti, A. Floris, G. Fratesi, G. Fugallo, R. Gebauer, U. Gerstmann, F. Giustino, T. Gorni, J. Jia, M. Kawamura, H.-Y. Ko, A. Kokalj, E. Küçükbenli, M. Lazzeri, M. Marsili, N. Marzari, F. Mauri, N. L. Nguyen, H.-V. Nguyen, A. Otero-de-la-Roza, L. Paulatto, S. Poncé, D. Rocca, R. Sabatini, B. Santra, M. Schlipf, A. P. Seitsonen, A. Smogunov, I. Timrov, T. Thonhauser, P. Umari, N. Vast, X. Wu, S. Baroni, Advanced capabilities for materials modelling with Quantum ESPRESSO, *J. Phys.: Condens. Matter* 29 (2017) 465901, www.quantum-espresso.org.
- 49 V. Eyert, The metal-insulator transitions of VO₂: A band theoretical approach, *Ann. Phys. (Leipzig)* 11 (2002) 650-702.
- 50 R.J.O. Mossaneck, M. Abbate, Optical response of metallic and insulating VO₂ calculated with the LDA approach, *J. Phys.: Condens. Matter* 19 (2007) 346225.
- 51 J.M. Tomczak, S. Biermann, Optical properties of correlated materials - Or why intelligent windows may look dirty, *Phys. Status Solidi B* 246 (2009) 1996-2005.
- 52 X. Yuan, Y. Zhang, T.A. Abteu, P. Zhang, W. Zhang, VO₂: Orbital competition, magnetism, and phase stability, *Phys. Rev. B* 86 (2012) 235103.
- 53 J. Zhang, H. He, Y. Xie, B. Pan, Theoretical study on the tungsten-induced reduction of transition temperature and the degradation of optical properties for VO₂, *J. Chem. Phys.* 138, (2013) 114705.
- 54 C. Sun, L. Yan, B. Yue, H. Liu, Y. Gao, The modulation of metal-insulator transition temperature of vanadium dioxide: a density functional theory study, *J. Mater. Chem. C* 2 (2014) 9283-9293.
- 55 H. Zheng, L.K. Wagner, Computation of the correlated metal-insulator transition in vanadium dioxide from first principles, *Phys. Rev. Lett.* 114 (2015) 176401.
- 56 J. Wan, Q. Ren, N. Wu, Y. Gao, Density functional theory study of M-doped (M = B, C, N, Mg, Al) VO₂ nanoparticles for thermochromic energy-saving foils, *J. Alloy. Compd.* 662 (2016) 621-627.
- 57 J.P. Perdew, K. Burke, M. Ernzerhof, Generalized Gradient Approximation Made Simple, *Phys. Rev. Lett.* 77 (1996) 3865-3868.

- 58 N. Marzari, D. Vanderbilt, M.C. Payne, Ensemble Density-Functional Theory for Ab Initio Molecular Dynamics of Metals and Finite-Temperature Insulators, *Phys. Rev. Lett.* 79 (1997) 1337-1340.
- 59 D. Vanderbilt, Soft self-consistent pseudopotentials in a generalized eigenvalue formalism, *Phys. Rev. B* 41 (1990) 7892-7895.
- 60 N. Troullier, J.L. Martins, Efficient pseudopotentials for plane-wave calculations, *Phys. Rev. B* 43 (1991) 1993-2006.